ELSEVIER

Cement & Concrete Composites 25 (2003) 131–143

Cement & Concrete Composites

www.elsevier.com/locate/cemconcomp

Modeling of structures subjected to impact: concrete behaviour under high strain rate

J.F. Georgin *, J.M. Reynouard

Civil Engineering Research Unit (URGC-Structures), National Institute of Applied Science (INSA of LYON), Villeurbanne 69621, France

Received 12 March 2001; accepted 18 September 2001

Abstract

This paper deals with a viscoplastic model which is the natural way to take into account the rate effect. Consideration of viscosity averts the habitual mesh sensitivity when strain softening is introduced by preserving the well-posedness of the initial boundary value problem. Modeling can constitute an alternative to experimentation not in order to predict the material response, but to try to understand and to evaluate the rate effect. Numerical simulation of the split test Hopkinson pressure bar gives an idea of dynamic concrete behaviour: forces of inertia, inertial confinement, structural effect and rate effect. Finally, the model is used to simulate a reinforced concrete beam submitted to impact.

Keywords: Finite element; Nonlinear analysis; Concrete; Viscoplasticity; Plasticity; Strain rate effect; SHPB; Dynamic loading

1. Introduction

The technological sophistication of our current industrial structures pushes us farther and farther take into account new loadings. Indeed, one cannot allow the construction of a nuclear power plant without considering the hazard of a falling plane or the risk of explosion. Consequently, understanding the behaviour of concrete subjected to fast loading such as impact or blast is essential. Experimentally, the response of a geomaterial such as concrete under impact loading is very difficult to capture. Moreover, several failure modes can be observed. A missile impact or an explosion on a concrete area can lead to local damage including perforation, scabbing, scaling and punching shear. Dynamic loading induces stress wave propagation in continuum media. The overall response of the structure must be considered. In this study, perforation striker are not taken into account because special numerical tools must be used such as remeshing. In the modeling of transient loading, it is very important to describe correctly the propagation velocity of the stress waves. In fact, the value of this velocity depends on the local material stiffness which is given by the material constitutive law. From the material point of view, concrete shows an increase in stiffness as the strain rate increases, a phenomenon called strain rate effect.

The modeling of the strain rate effect in concrete is not very easy to tackle. A mathematical model is useful in order to describe the observed material behaviour such as strain rate only when we have a well-understood phenomenon. In the literature, many authors have put forth several possible rate effect explanations; free water [1–3,17,23], friction effect [13] or confinement by inertial lateral restraint [22]. The current belief is the following; the increase of strength for strain rate under 1 s^{-1} comes from free water (Stefan effect), and for strain rate over 10 s^{-1} from forces of inertia. Using these assumptions, numerical simulation can be a tool towards gaining greater insight into the dynamic behaviour of concrete.

In this study, simulation of the dynamic compressive test using the split Hopkinson pressure bar (SHPB) is performed. Available experimental data were found in the works of Gary [9]. In recent years, many works have been carried out on the problem of wave propagation in softening materials such as geomaterials. The localization failure process of the softening material described by a classical continuum approach may bring to light an

* Corresponding author.
E-mail address: Jean-Francois.Georgin@insa-lyon.fr (J.F. Georgin).

0958-9465/03/$ - see front matter
PII: S0958-9465(01)00060-9

ill-posed problem, non uniqueness and loss of stability. In the literature, a few solution techniques have been suggested to preserve the well-posedness of the problem. In particular, a rate-dependent model gives the existence, the uniqueness and the mesh independence of numerical results. Sluys and De Borst [21] has demonstrated that viscosity enhances regularization effect. Modeling of concrete which is a softening material by a classical model in the finite element method (FEM) can lead to mesh-dependent numerical response. Accordingly, improvement given by a rate-dependent concrete model is discussed here.

The focus of this paper is to evaluate the ability of a static concrete based model to describe dynamic concrete behaviour. In the first part, an elastic–viscoplastic concrete model used in this work is presented. The following part concerns the localization problem in the FEM. We emphasize the necessity to use viscosity as a technique of regularization in numerical dynamic calculation. Third, a comparison between simulation results and experimental data from the SHPB test leads to a discussion about the strain rate effect in the concrete material. The final part concerns the structural validation of the concrete model through the comparison of the model prediction and experimental observations of an impacted reinforced concrete beam.

2. Concrete model

Representation of cracking behaviour is the main difficulty in modeling of concrete and reinforced concrete. Many finite element programs have adopted the smeared crack concept for dealing with this tension behaviour where relative displacements of crack surfaces are represented by crack strains and the constitutive behaviour of cracked concrete is modeled in terms of stress–strain relations. Contrary to the discrete crack concept, the smeared crack concept preserves the nature of the finite element displacement method because the continuity of the displacement field remains intact. Nevertheless, on the one hand, combination of fixed-crack with plasticity can lead to numerical difficulties as shown by Wang et al. [24] and on the other hand, we can have an overestimation of the failure load with fixed smeared crack model [5].

Feenstra [8] suggested a constitutive model which describes the formation of cracks within the framework of plasticity. The concrete model proposed and implemented in CASTEM 2000 code [4] is based on the works of Feenstra [8] with regard to cracked concrete. The model was validated by Georgin [10] in the case of static loads using data from some tests involving rheological and structural behaviour. Hypotheses commonly used in the theory of plasticity are assumed: strains partition,

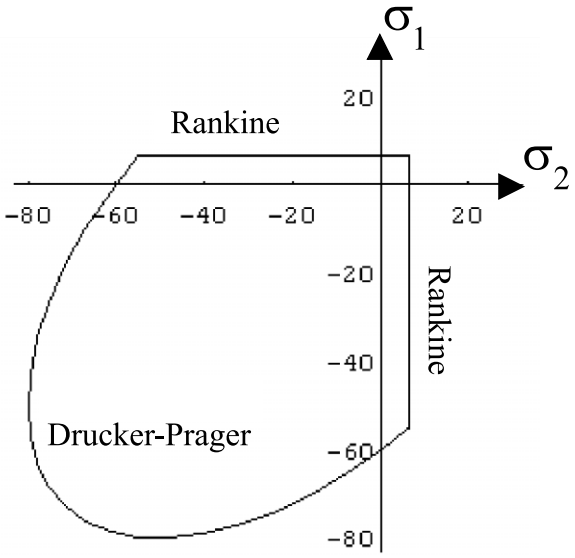

Fig. 1. Non-smooth yield criteria.

associated flow and isotropic hardening. In order to represent correctly the asymmetrical material behaviour in tension and compression, we define a non-smooth yield criterion (Fig. 1). The simple Rankine criterion (f_1) is used to define the tension behaviour of the material in the major principal stress direction. The behaviour in the second principal direction is deduced by Mohr circle considerations. The biaxial compression is modelled either by the Von-Mises criterion (f_2), or by the Drucker–Prager criterion (f_2). The originality comes from the fact that the tension behaviour is also modelled on the basis of plasticity. Cracked material is modeled by a continuum description. A stress–strain material law similar to the compression stress–strain law is used to represent tension behaviour. At the multi-surface criterion corner, the ambiguity of plastic flow direction is removed according to the proposal by Koiter [12] and Maier [14] by considering the contribution of each individual loading surface (Fig. 2)

$$\{\dot{\varepsilon}^{\mathrm{p}}\} = \dot{\lambda}_1\{\partial_\sigma f_1\} + \dot{\lambda}_2\{\partial_\sigma f_2\}, \tag{1}$$

wherein $\{\dot{\varepsilon}^{\mathrm{p}}\}$ is the plastic strain rate vector, $\dot{\lambda}_{\mathrm{i}}$ is the plastic multiplier and ∂_σ is the derivative of the criterion f_{i} with respect to the stress vector $\{\sigma\}$.

The algorithm of plasticity is the typical trapezoidal Euler backward scheme used by Simo [19] and further developed by Feenstra [8] (Fig. 3). The plastic stress vector is obtained by solving the updated stress equation

$$\{\sigma\}^{(i)} = \{\sigma_{\mathrm{e}}\} - [D_{\mathrm{e}}].\Big\{\Delta\lambda_1^{(i)}\{\partial_\sigma f_1\}^{(i)} + \Delta\lambda_2^{(i)}\{\partial_\sigma f_2\}^{(i)}\Big\}, \tag{2}$$

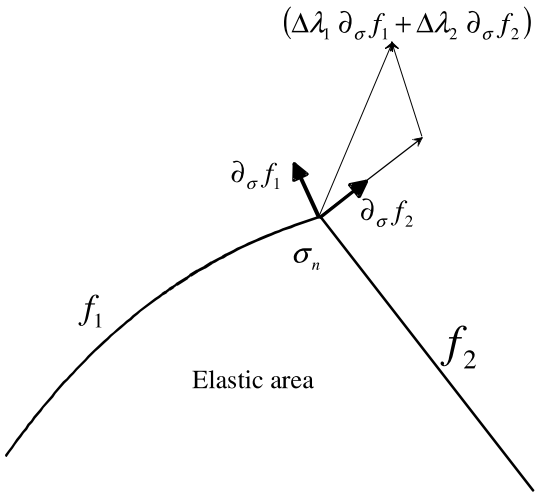

Fig. 2. Contribution of each surface at the corner.

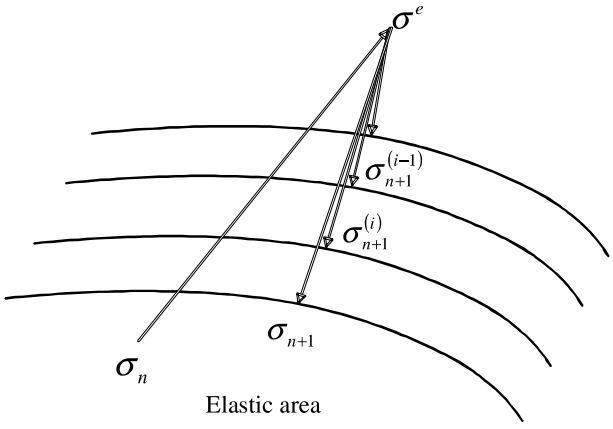

Fig. 3. Return mapping.

wherein $[D_e]$ corresponds to the Hookean elastic matrix and $\{\sigma_e\}$ is the predictor stress vector.

Then, all the procedure consists of determining the inelastic incremental multipliers which enforce the plasticity condition

$$\begin{aligned} &f_1(\Delta\lambda_1,\ \Delta\lambda_2)=0,\\ &f_2(\Delta\lambda_1,\ \Delta\lambda_2)=0. \end{aligned} \tag{3}$$

A Newton–Raphson method is used to solve this iterative process. We calculate the updated inelastic incremental multiplier with

$$\begin{aligned} &\begin{Bmatrix}\Delta\lambda_1\\ \Delta\lambda_2\end{Bmatrix}^{(i+1)}=\begin{Bmatrix}\Delta\lambda_1\\ \Delta\lambda_2\end{Bmatrix}^{(i)}-J_i^{-1}\begin{Bmatrix}f_1\\ f_2\end{Bmatrix}^{(i)},\\ &J_i=\begin{bmatrix}\frac{\partial f_1}{\partial\lambda_1} & \frac{\partial f_1}{\partial\lambda_2}\\ \frac{\partial f_2}{\partial\lambda_1} & \frac{\partial f_2}{\partial\lambda_2}\end{bmatrix}_i \end{aligned} \tag{4}$$

wherein the Jacobian J_i is comprised of the partial derivatives of criteria with respect to the plastic multipliers [16]. The latter is determined with a Broyden method. In the case of a single criterion, the Broyden updated Jacobian matrix is a secant method. But, this can lead to numerical divergence. Then, one can optimise the iterative process; after a certain number of iterations, if plastic convergence is not obtained another method as for example the tangent method is used.

The extension of the plastic model to the viscoplastic model is achieved with the help of the Duvaut–Lions viscoplasticity theory

$$\{\dot\varepsilon^{vp}\}=\frac{1}{\eta}[D_e]^{-1}\{\{\sigma\}-\{\sigma_p\}\}. \tag{5}$$

Now, we assume the partition of the total strain rate vector into an elastic strain rate vector and a viscoplastic strain rate vector

$$\{\dot\varepsilon\}=\{\dot\varepsilon^{e}\}+\{\dot\varepsilon^{vp}\}. \tag{6}$$

The formulation of this viscous model allows non smooth multisurface criterion to be used in contrast to the Perzyna model. The uniaxial representation of this viscoplastic model is shown in Fig. 4. First of all, the resolution of the constitutive equations is carried out considering the material as rate independent (we consider solely the lower branch in Fig. 4). Then the "plastic" stress tensor $\{\sigma_p\}$ and a hardening variable κ_p are obtained. In the second phase, we consider the rate-dependent model by using the Duvaut–Lions relationship in Eq. (5), η is a viscosity parameter, $\{\dot\varepsilon^{vp}\}$ is the viscoplastic strain rate vector and $\{\sigma\}$ is the stress vector at time t. The viscoplastic hardening rate parameter $\dot\kappa$, is given in a similar fashion as follows:

$$\dot\kappa=-\frac{1}{\eta}(\kappa-\kappa_p). \tag{7}$$

After solving the differential equations (5) and (7), we obtain the updated viscoplastic stress vector, Eq. (8) and the updated viscoplastic rate parameter, Eq. (9) as Simo [19] presented, where $t+\Delta t$ is the time at the end of the calculation step and t is the beginning of the step, $\{\Delta\varepsilon\}$ is the incremental strain vector in the step. As Sluys [20]

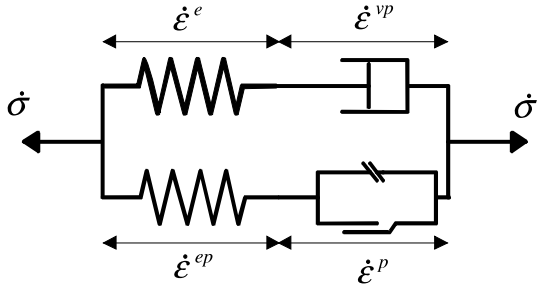

Fig. 4. Uniaxial model description.

discussed, this solution does not provide a stress–strain matrix which is needed for use in the implicit time integration scheme. We can use this technique because to simulate dynamic loadings, an explicit central difference time integration scheme is implemented in the CASTEM 2000 code. Accordingly, a consistent tangent matrix is not necessary with this time discretization.

$$\{\sigma\}^{t+\Delta T} = \{\sigma\}^{t}\left(e^{-(\Delta t)/\eta}\right) + \left(1 - e^{-(\Delta t)/\eta}\right)\{\sigma_p\} + \left(\frac{1 - e^{-(\Delta t)/\eta}}{\Delta t/\eta}\right)[D_e]\{\Delta\varepsilon\}, \tag{8}$$

$$\kappa^{t+\Delta T} = \kappa^{t}\left(e^{-(\Delta t)/\eta}\right) + \left(1 - e^{-(\Delta t)/\eta}\right)\kappa_p. \tag{9}$$

One can remark that the elastic case is recovered if $\Delta t/\eta \to 0$ and that the rate independent plastic case is recovered if $\Delta t/\eta \to \infty$.

3. Localisation problem

Fracture process in quasi-brittle materials cannot be described with a standard rate-independent model. When a material is so heavily damaged, non-homogeneous deformations occur at the micro-structure level. The inadequacy of the classical description is due to the fact that we obtain a stress–strain curve only by dividing the force and the elongation by the original load-carrying area and the original length of the specimen, respectively. In this process, we assume homogeneous deformations. The classical mathematical description leads to unreliable numerical results. Indeed, the appearance of the softening in the material law leads to a loss of uniqueness of the solution. In statics, the equations become hyperbolic and in dynamics, they become elliptic. Without specific processing, the description of the classic continuum does not permit the physical phenomenon of strain localisation to be simulated. To solve this problem, we must introduce additional terms in the continuum description which take into account modifications at the micro-structure level during the fracture process. In the literature, there are several technical solutions in order to enrich continuum description by adding higher-order terms either in space or in time. Sluys [20] presented all these methods. The fracture energy model was developed for mode I failure. The Cosserat continuum model is useful for mode II dominated localisation problems. In gradient model, spatial derivatives of the inelastic state variables enable non-homogeneous failure to be described correctly. A rate-dependent model with introduction of higher-order time derivatives preserves the character of equations. In our dynamic problem, the viscosity solution seemed the most appropriate solution to keep the problem well-posed.

Considering an uniaxial wave propagation, the equation of motion in a classical description is

$$\left(\frac{E + f'}{c_e^2}\right)\left(\frac{\partial^2 \dot{u}}{\partial t^2}\right) - f'\left(\frac{\partial^2 \dot{u}}{\partial x^2}\right) = 0, \tag{10}$$

wherein E corresponds to the Young modulus, c_e is the elastic wave celerity, f' is the slope of the plastic curve, u is the displacement of a particle x at time t. We can clearly observe that the beginning of softening ($f' < 0$) transforms the equation character. Then, the velocity of longitudinal wave becomes imaginary. Introducing first-order viscoplastic strain rate dependence allows characteristics in the plane (x, t) to be real, Eq. (11)

$$m\left(\frac{1}{c_e^2}\frac{\partial^3 \dot{u}}{\partial t^3} - \frac{\partial^3 \dot{u}}{\partial x^2 \partial t}\right) + \left(\frac{E + f'}{c_e^2}\right)\left(\frac{\partial^2 \dot{u}}{\partial t^2}\right) - f'\left(\frac{\partial^2 \dot{u}}{\partial x^2}\right) = 0. \tag{11}$$

The study of the dispersion shows that a viscoplastic medium is dispersive in contrast to an elastic medium which is non-dispersive. A dispersive material can transform a travelling wave group, because in a classical dispersive system, waves of low frequency travel faster than those of high frequency. Fig. 5 shows this phenomenon. Moreover, the harmonic solution to Eq. (11) can be written as

$$\dot{u} = A e^{-\alpha x} e^{i(k_r - \omega t)}, \tag{12}$$

wherein α is a damping coefficient, k_r is the wave number, ω is the radial frequency of wave. Fig. 6 shows the dependency of the damping coefficient on the radial frequency. From a localization point of view, this property is very important. We can infer from Fig. 6 that the damping coefficient for high frequencies provides localization of deformation. Indeed, the coefficient α has a mathematical limit viz

$$\lim_{\omega \to +\infty} \alpha^{-1} = l, \tag{13}$$

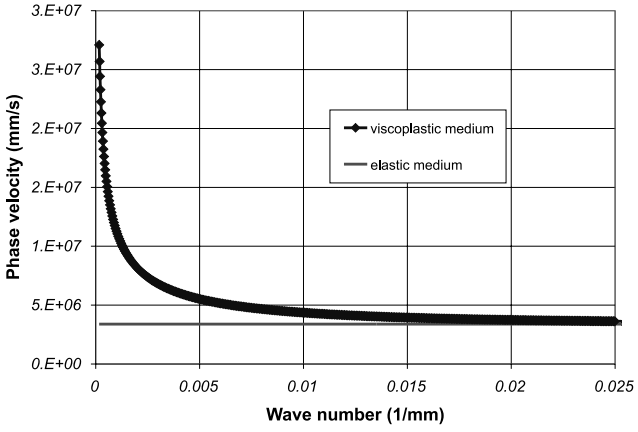

Fig. 5. Phase velocity versus wave number.

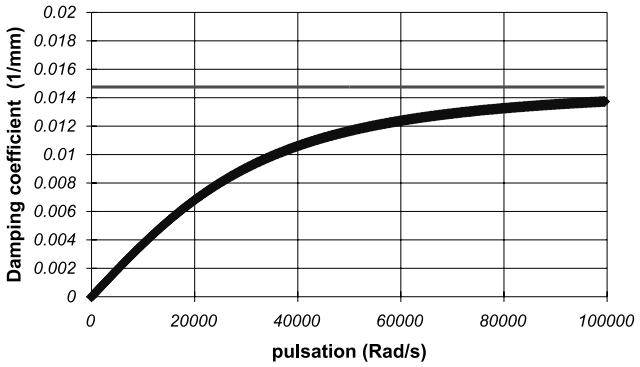

Fig. 6. Damping coefficient versus radial frequency.

where l can be viewed as the characteristic length. For Duvaut–Lions viscoplasticity model, by analogy with a rate-dependent model, the characteristic length is for a mode I failure

$$l = 2\eta c_e. \tag{14}$$

Regularisation effect and mesh independence effected by viscoplastic model can be demonstrated by means of a one-dimensional bar. A bar is fixed at one end and is loaded by a dynamic tensile force at the other end. The geometry of the problem and the loading diagram are given in Fig 7. The transient wave propagates through the bar and reflects at the left boundary. If the stress which is imposed at one end is as $0.5f_t < q < f_t$, the tensile strength f_t is exceeded after the reflection wave and a localized softening zone emerges. Fig. 8 shows that viscosity can develop localization in a finite length

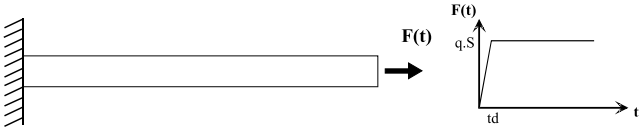

Fig. 7. Geometry and loading description.

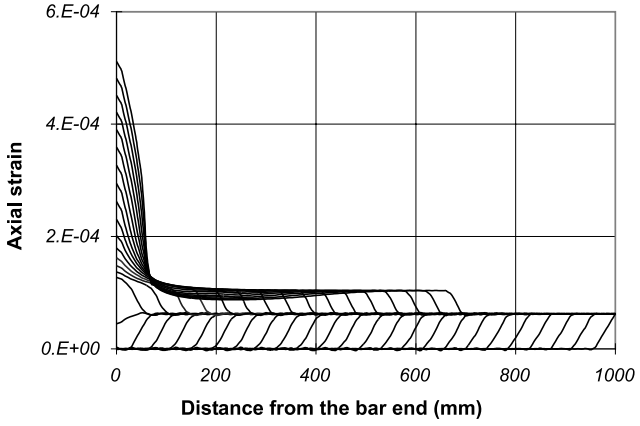

Fig. 8. Strain wave evolution (with viscosity).

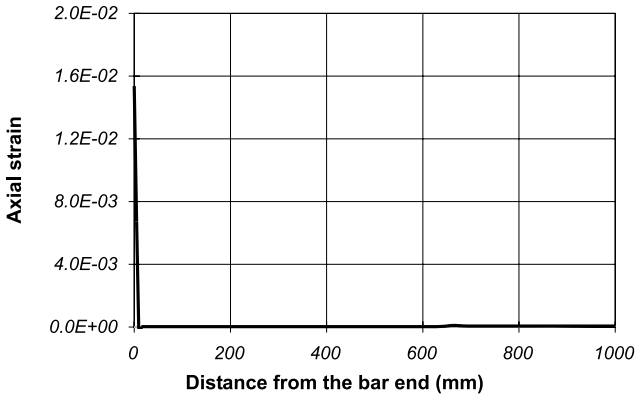

Fig. 9. Strain wave evolution (without viscosity).

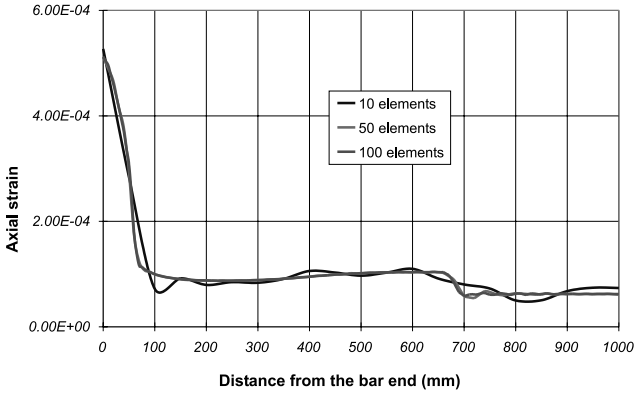

Fig. 10. Mesh independence (with viscosity).

in opposition to the plastic model in Fig. 9. With a plastic model, wave propagation velocity is imaginary in softening regime. Energy is dissipated on zero length zone. Higher frequencies are attenuated and then do not disturb the travelling wave. Finally, viscosity brings a mesh independence as Fig. 10 shows. Viscoplastic model leads to one result only with several meshes whereas plastic model gives different pic-strain with different meshes (Fig. 11).

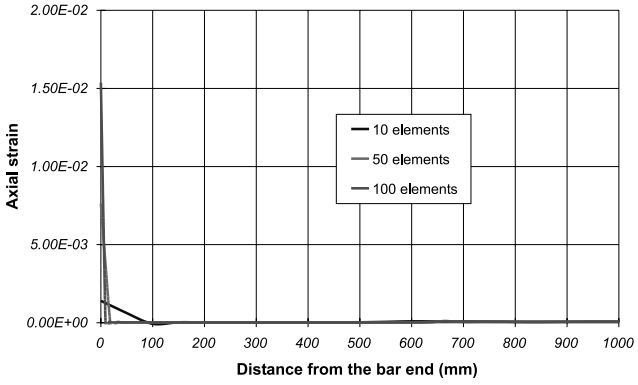

Fig. 11. Mesh dependence (without viscosity).

4. Modeling of concrete under dynamic loading

4.1. Rate effect

The question which must now be addressed is the following: what is the origin of the strain rate effect observed in the experimental dynamics loadings test on the concrete material and how must we take it into account in the numerical modeling?

From the previous discussion, one finds that many attempts have been made to explain the observe behaviour. The numerical simulation by the finite elements method is useful tool to obtain more insight into the strain rate effect. Indeed, modeling of a concrete specimen under high strain rate can give some idea about the transient dynamic concrete behaviour. Influent parameters can be identified from the numerical calculation as, rheology with viscoplasticity, the contribution of forces of inertia and structural effect resulting from boundary restraints. In the first place, the viscosity contribution to the strain rate is emphasized. Static simulation on one finite element with one-point Gaussian integration brought to light the material rate effect of the model. Let us recall that the parameter of viscosity is bound by the characteristic length of the material which is a reasonable datum for defining the microscopic behaviour of concrete on a macroscopic scale. Sensitivity to strain rate is presented in Figs. 12 and 13 for compression and tension, respectively. The strength increase is compared with experiments reported by Bischoff and Perry [3] for compression and by Toulemonde [23] for tension. Figs. 14 and 15 show this comparison for compression and tension, respectively. We note that the viscosity parameter cannot be considered independent because it is mathematically linked with the characteristic length, Eq. (12). We can observe that the rate effect behaviour underestimates experimental results. Consequently, we hope that inertial contribution will be sizeable.

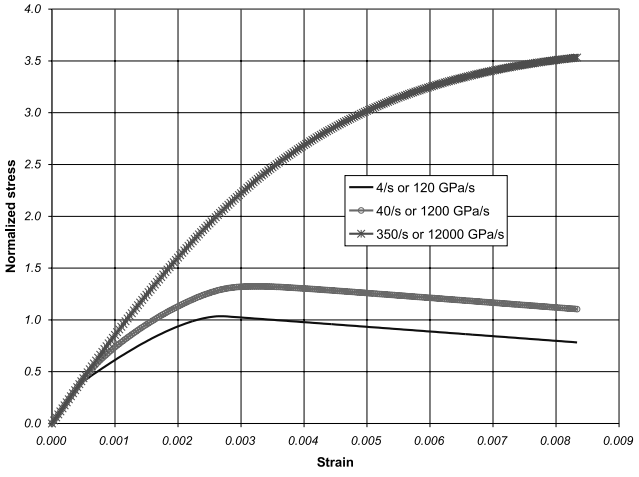

Fig. 12. Material strain rate effect on compressive behaviour.

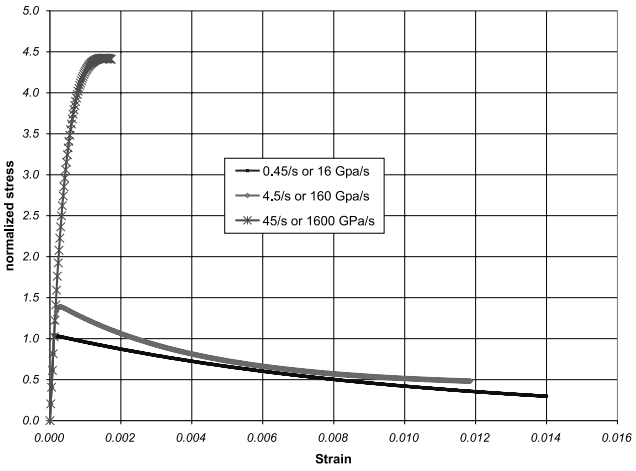

Fig. 13. Material strain rate effect on tensile behaviour.

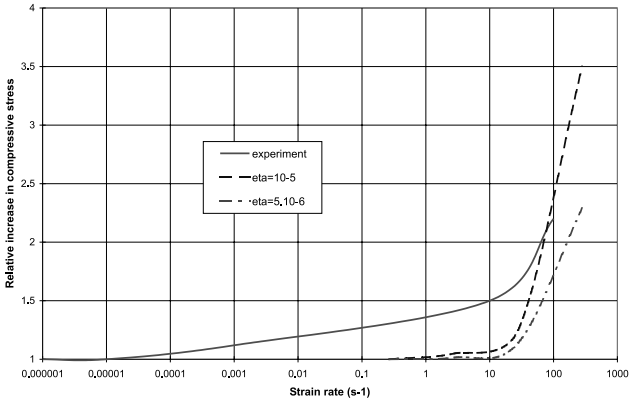

Fig. 14. Strain rate in compression.

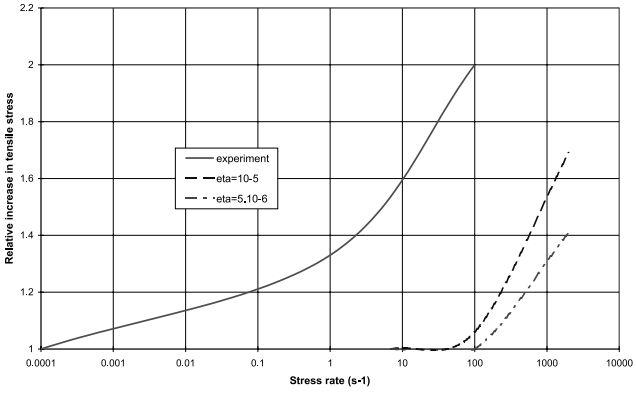

Fig. 15. Strain rate in tension.

Fig. 12 put in a prominent manner a inconsistent physical point in the response given by this approach. Indeed, the ductility behaviour of the model response does not decrease with the increase of the strain rate as

observed in the experiments. This property could be introduced in the modelling by taking into account the dependency of fracture energy with strain rate. Nevertheless, the aim of this work is concerning the strength evolution.

4.2. Simulation of the Hopkinson pressure bar test

The split Hopkinson pressure bar technique (SHPB) has been known for a long time [11]. The SHPB test enables the dynamic behaviour of many different materials to be investigated. Figs. 16 and 17 illustrate the experimental set-up where the principal device consists of a projectile, an instrumented input bar, an instrumented output bar and a short material specimen.

Missile impacts the input bar and creates a compression stress wave which propagates through the input bar, pierces the specimen and propagates again in the output bar. At the boundaries between the specimen and the input and output bars, the stress is partially refracted and partially reflected in relation to the corresponding mechanical impedances and cross-sectional areas. The specimen breaks after several reflections of waves inside it. Measurements are made on the two elastic bars and transported in time to the interfaces with the test specimen. But the classical SHPB method is based on the assumption that stress and strain fields in the specimen are at any given instant one-dimensional, uniform over the cross-section and in the axial direction. This is true for homogeneous material, for heterogeneous materials like concrete, the SHPB validity has been proven by Zhao and Gary [25]. A special procedure enables the input and the output strain waves versus time to be obtained. So that, the forces and velocities are given by the following relations:

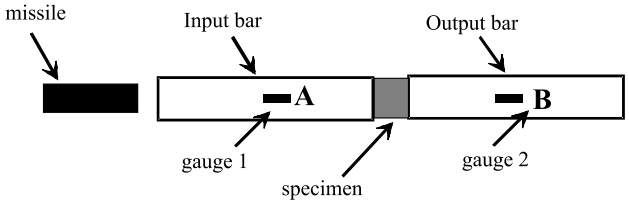

Fig. 16. SHPB description.

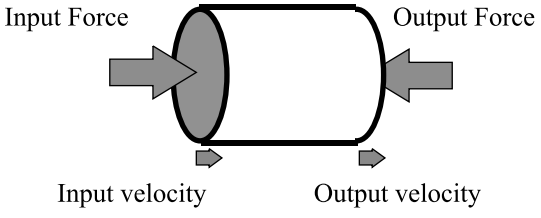

Fig. 17. Boundary conditions.

$$F_{\text{input}} = AE(\varepsilon_{\text{i}} + \varepsilon_{\text{r}}), \tag{15}$$

$$F_{\text{output}} = AE(\varepsilon_{\text{t}}), \tag{16}$$

$$V_{\text{input}} = C(\varepsilon_{\text{i}} - \varepsilon_{\text{r}}), \tag{17}$$

$$V_{\text{output}} = C(\varepsilon_{\text{t}}), \tag{18}$$

wherein A is the cross-section area of the elastic bars, E the Young's modulus of the elastic bars, $C = \sqrt{E/\rho}$ the wave velocity in elastic medium, ρ the density of the elastic bar, ε_{i} the input strain wave in input elastic bar, ε_{r} the reflected strain wave in input elastic bar and ε_{t} is the output strain wave in the output elastic bar.

We can estimate consequently the average strain rate and the average stress which is imposed on the specimen with:

$$\dot{\varepsilon}_{\text{S}} = \frac{V_{\text{output}} - V_{\text{input}}}{l_{\text{S}}}, \tag{19}$$

$$\sigma_{\text{S}} = \frac{F_{\text{input}} + F_{\text{output}}}{2A_{\text{S}}}. \tag{20}$$

Experiments on several samples at different strain rates and confinements have been carried out by Gary [9] in the framework of the "GRECO géomatériaux" project. The tested specimens are cylindrical. The geometrical characteristics are either diameter 36 mm with length 36 mm or diameter 30 mm and length 40 mm. We show a sample of these measurements from one test (36 × 36) in Figs. 18 and 19, showing forces and velocities, respectively.

We simulated this test with the proposed viscoplastic model in order to evaluate the material concrete behaviour. In modeling of transient loading, it is very important to describe correctly the propagation velocity of stress wave. The value of this velocity depends on the local stiffness of the material which is given by the material constitutive law. The simulations input data are the recorded experimental velocities, whereas the simulation output data are the computed forces that are compared with the experimental ones.

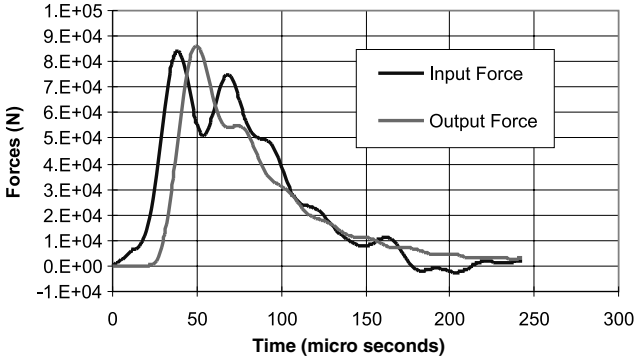

Fig. 18. Experimental forces.

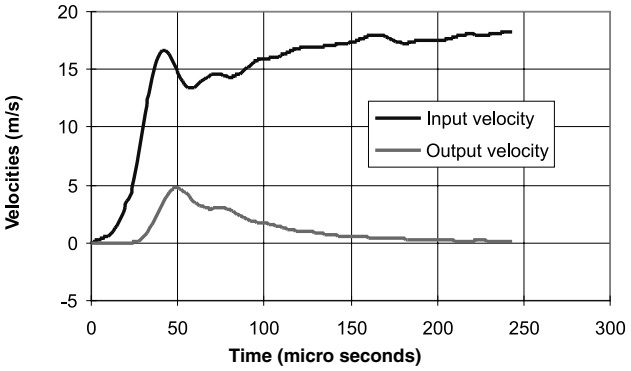

Fig. 19. Experimental velocities.

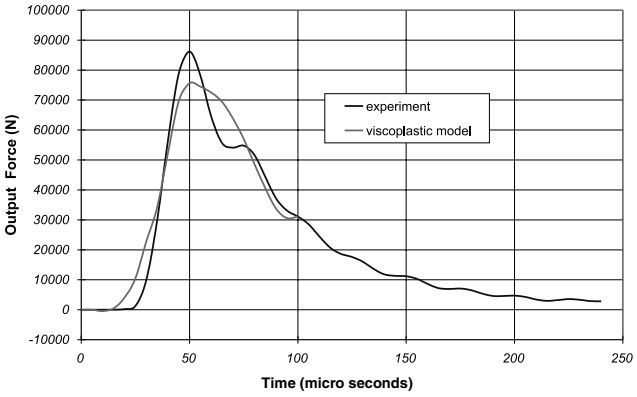

Fig. 21. Output force (Drucker–Prager).

Dynamic and inertial terms are integrated in equilibrium equations. In this simulation, only the concrete specimen is considered. Numerical description of the specimen is axisymmetrical. Simulation was done with a viscosity parameter $\eta = 2 \times 10^{-6}$ which corresponds to a characteristic length of 12 mm (micro concrete), and fixed or free radial boundary conditions. The physical behaviour of the specimen is to be marked out by the two extreme assumption of boundary conditions. There is unknown friction between the sample and the elastic bars. But, the free boundary conditions study will be carried out later. Parameters to be introduced in the model are very simple to estimate: Young's modulus $E = 23{,}000$ MPa, compressive strength $f_c = 50$ MPa, tensile strength $f_t = 5$ MPa, the fracture energies $G_t = 0.1$ N mm/mm^2 and $G_c = 5$ N mm/mm^2.

The analysis which is presented in this paper was carried out using a 24×24 mesh of four-noded plane elements with four-point Gaussian integration. Calculation was also performed with three other meshes: 16×8, 32×16 with four-noded plane elements and 32×16 with three-noded plane elements in order to check the mesh independence. The numerical results for the experiments at 450 s^{-1} are plotted in Figs. 20 and 21 in terms of input forces and output forces versus time. Although the input force which is given by the model overestimates the experimental input force and the output force underestimates the experimental output force, the numerical results are quite satisfactory. The static force of 60,000 N which could be supported by the specimen is exceeded in this dynamic test by 30 percent.

The state of hydrostatic pressure inside the sample can explain the increase in strength because the concrete material is pressure-dependent. A confinement can be provided by an inertial effect (inertial confinement) or by boundary conditions (structural effect). This numerical simulation shows that at the core of the sample, the model gives a level of hydrostatic pressure of about 46 MPa and in this case we used a Drucker–Prager plastic surface. Numerically, it is possible to bring to the fore the increase of stress provided by pressure dependence by using a Drucker–Prager or a Von-Mises plastic surface. Figs. 22 and 23 show a comparison between the experimental and the simulation results in the latter case. The model response with the Drucker–Prager versus the Von-Mises is quite different. For the Von-Mises model, output force does not increase and the input force is always bigger than the static force although the maximum force decreases compared with the

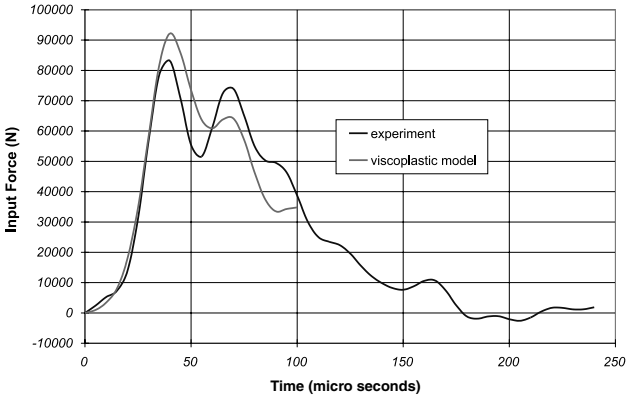

Fig. 20. Input force (Drucker–Prager).

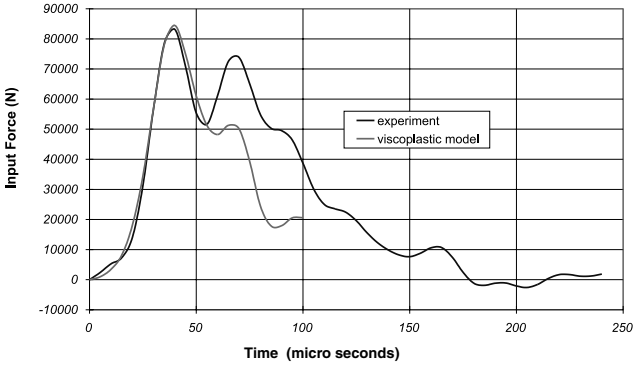

Fig. 22. Input force (Von-Mises).

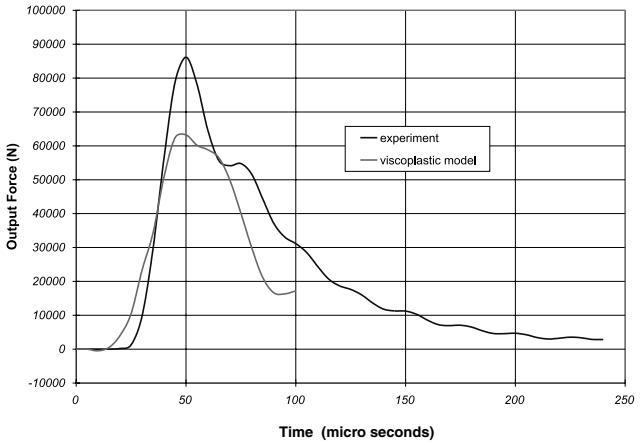

Fig. 23. Output force (Von-Mises).

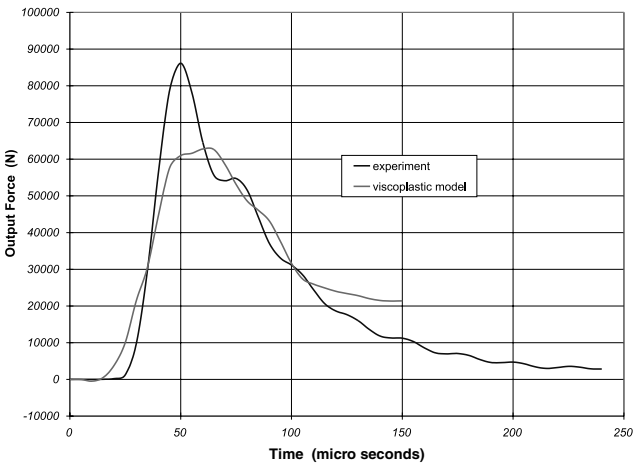

Fig. 25. Output force (Drucker–Prager) free radial boundary conditions.

Drucker–Prager. For this reason, we can say that confinement contributes to increasing strength in this range of strain rate. However, we do not know if this confinement comes from inertial effect or from structural effect.

Now, we consider the structural behaviour of the specimen. The aim of the experimental testing is to verify the material law which will be useful for a local model. Yet, the boundary conditions of the specimen can also lead to an increased apparent strength in static and dynamic. In the SHPB test, it is difficult to evaluate the shear stress state imposed at the end zones by frictional restraints resulting from the interaction between the specimen and the elastic bars. In previous simulation, we imposed fixed radial displacement at the ends of the specimen. Now we simulate testing with free radial displacement at the extremities. Of course, the real behaviour is between these two extreme cases.

The pressure-dependent (Drucker–Prager) viscoplastic model gives the response which is plotted in Figs. 24 and 25. The output force does not increase while the input force increases. At the core of the sample, hydrostatic pressure does not exceed 20 MPa. This result shows that a structural effect can contribute partially to the confinement inside the sample and consequently to the strain rate effect. Nevertheless, one can imagine that an inertial effect is involved in the phenomenon of the rate effect brought into play by the lateral inertial confinement. In the free radial displacement configuration, only the input force is modified. The deformed shapes of the specimen, Figs. 26 and 27, can help to explain the contribution of inertial confinement and of the structural effect. In the second case (Fig. 27), the first half of the specimen is submitted to high lateral strains which lead to forming a resilient cone. For that matter, we can state that the cone development is bigger in the first case (Fig. 26) at the two contact ends. The plastic deformations are not homogeneous and tend to propagate from the lateral free surfaces to the core of the sample. Fig. 28 shows the contours of the hardening damage of the

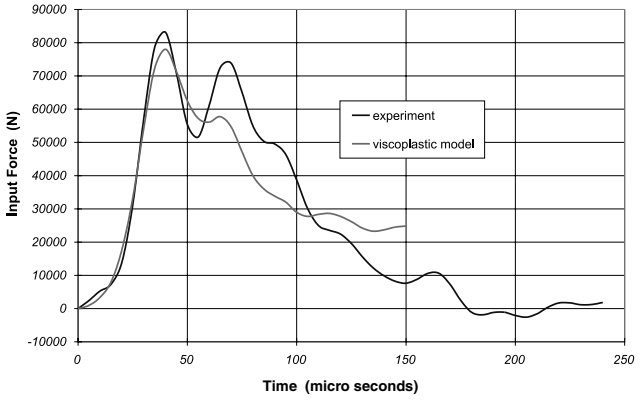

Fig. 24. Input force (Drucker–Prager) free radial boundary conditions.

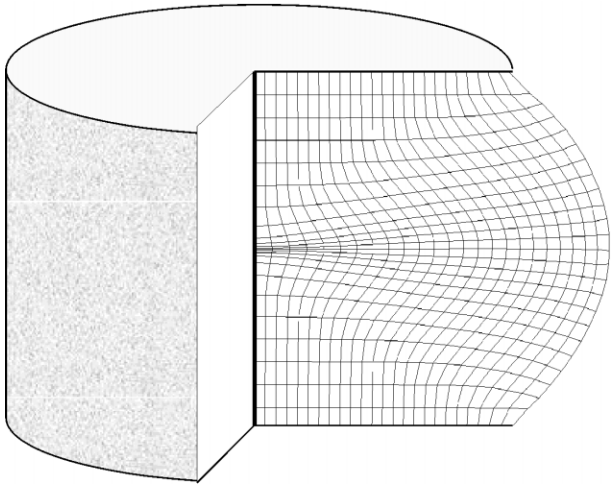

Fig. 26. Deformed shape (fixed radial boundary conditions).

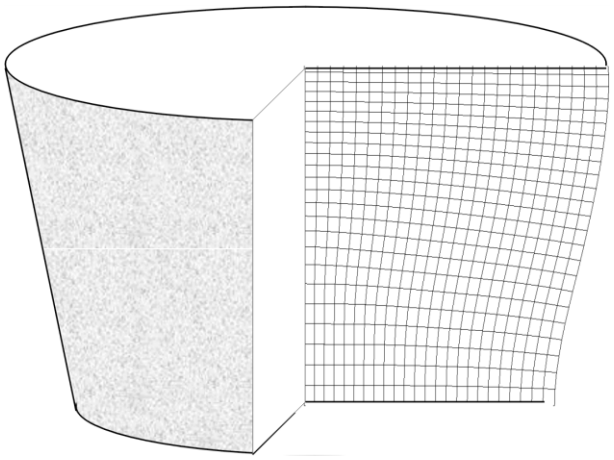

Fig. 27. Deformed shape (free radial boundary conditions).

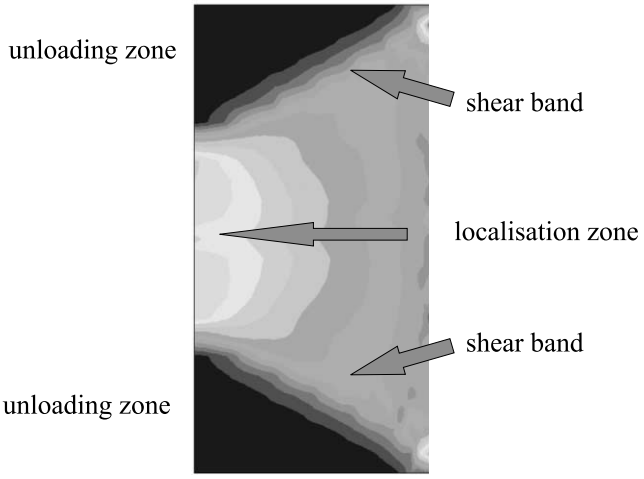

Fig. 28. Diagram hardening variable in compression (fixed radial extremities).

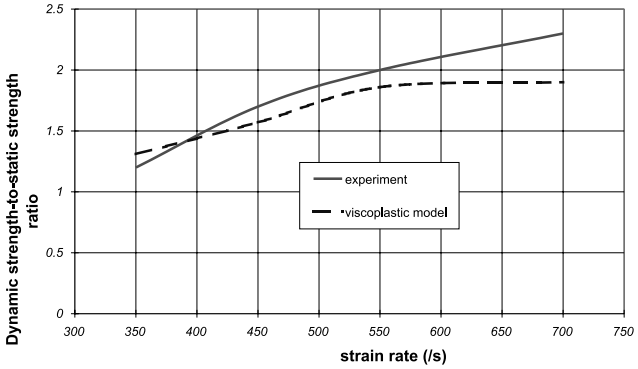

Fig. 29. Influence of strain rate without radial confinement.

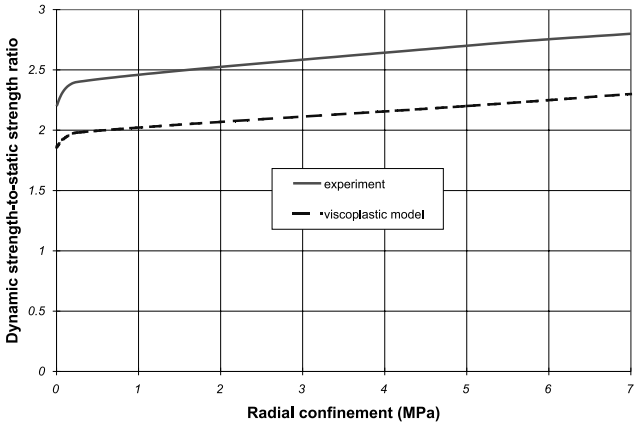

Fig. 30. Influence of radial confinement strain rate of 700 s^{-1}.

material. We notice a strong damage zone which is in the middle of specimen and at the beginning of the specimen with free radial ends displacement. Moreover, shear bands and unloading zones appear in the specimen. We can see then that the viscoplastic model can describe localization of the deformation on a finite length. This test corresponds to a 450 s^{-1} strain rate. One can say that the external zone damages itself progressively while the core remains for a certain time elastic due to the effect of inertial confinement.

Consequently, similar to Rossi [17], we showed that for high strain rate, inertial behaviour is important in the response of the material. It is difficult to say that this test completely describes the intrinsic property of the concrete under dynamic loading. These explanations concern numerical results but we can say that experimentally, inertial confinement and forces of inertia are also present.

Gary carried out several experiments using the SHPB test in order to study the dependence of both strain rate and lateral pressure on the strength. He produced a list of all measurements in terms of force and velocity. We simulated a whole range of tests and noticed the mean of the input and output force. In the simulation, fixed radial displacement at the ends of the sample and the viscoplastic model pressure-sensitive model is employed. The evolution of strength versus strain rate or confinement is shown in Figs. 29–31. The model describes correctly the variation of relative increase of compressive strength although the numerical results underestimate the experimental results. The output force is always less than the experimental one as we saw previously and we have reported the mean value between the input and the output force. Nevertheless, the finite element calculation provides a material behaviour simulation which is in satisfactory agreement with the observed behaviour in tests.

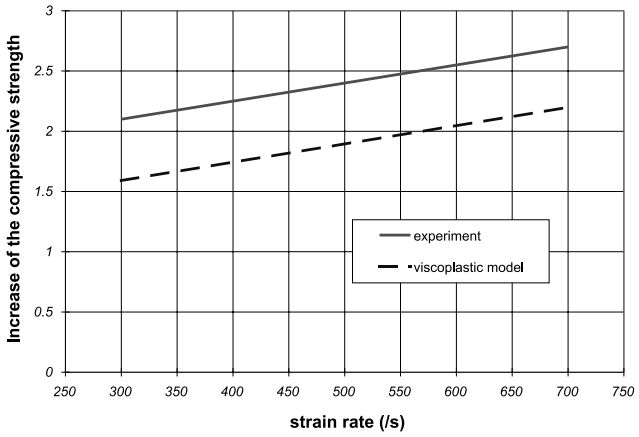

Fig. 31. Influence of strain rate with radial confinement of 5 MPa.

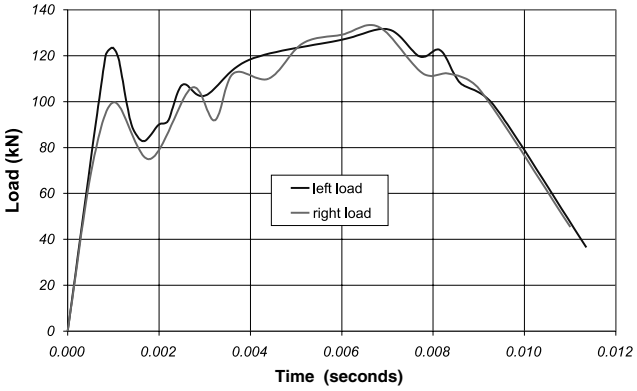

Fig. 33. Loading history.

5. From material behaviour to structure

In this part, we extended the viscoplastic material description to the simulation of structures subjected to impact. Impact testing on a steel fibre reinforced concrete beam was carried out at the Institute für Massivbau und Baustofftechnologie in Karlsruhe University [7]. The aim of the research was to determine the influence of the addition of fibres to the impact resistance of a reinforced concrete.

Many computations on this beam were performed with a rate-dependent smeared crack model by Sluys and De Borst [21], with a rate-dependent damage model by Dubé et al. [6] and with a gradient-dependent plasticity model by Meftah [15]. Fig. 32 shows the beam geometry. It is a concrete beam reinforced by four steel bars and steel fibres. We can see in Fig. 33 the loading history for the left and the right loads recorded during the experiment. In contrast to the calculation of Sluys et al. [21], in this study as well as in others, we have assumed that the supports are perfectly rigid. The material characteristics are $E = 32{,}940$ MPa, compressive strength $f_c = 31.5$ MPa, tensile strength tension $f_t = 3.15$ MPa, the fracture energies $G_t = 0.1$ N mm/mm^2 and $G_c = 3$ N mm/mm^2 and the characteristic length for concrete in contrast to micro concrete, which corresponds to $\eta = 2 \times 10^{-5}$ s. A calculation was carried out with a viscoplastic model using discrete Kirchhoff finite element formulation. This type of finite element for plate and shell is based on the equivalent assumption of Euler–Navier Bernouilli for the beam. In others words, shearing behaviour is not taken into account. Each plate is subdivided into layers whose behaviour is two-dimensional (plane stress state). Because in a beam, transversal behaviour is insignificant, this modeling is equivalent to one-dimensional model. Fig. 34 shows the response of the model in comparison with experiment and other models in term of displacement recorded at midspan. The calculate results agree well with the experimental data and with previous simulations. Moreover, the failure mode is a first-order vibration mode as we could observe in the experimentation.

Fig. 35 shows the comparison between a calculation with the viscoplastic model and an elastic model. The response of the elastic model is stiffer than the viscoplastic one. Although deflections are of the same order of accuracy, the non-linear model gives cracked and highly compressed zones in the beam which are not replicated by the elastic model. We can see in Figs. 36 and 37 the damage zones in tension and compression, respectively. Plastic deformations take place in several elements. Further, the viscoplastic model estimation of the evolution of the left support reaction of the beam is

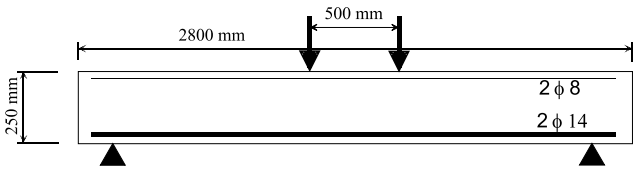

Fig. 32. Geometry description.

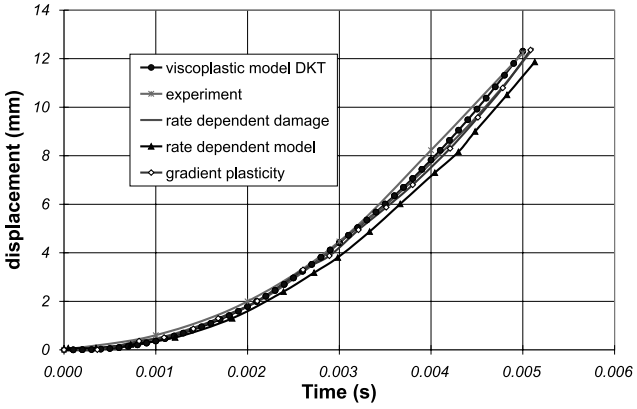

Fig. 34. Comparison of various constitutive models predictions with experimentally measured displacements.

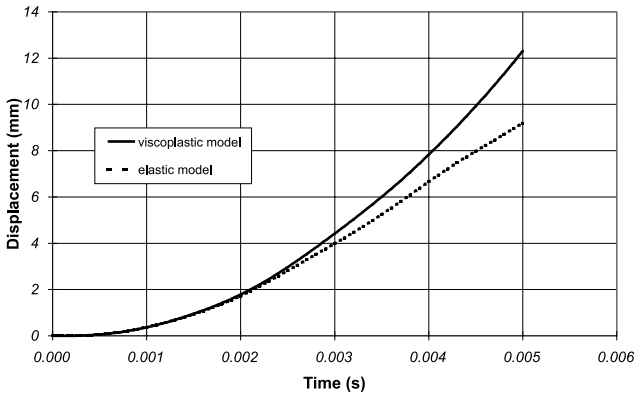

Fig. 35. Comparison between elastic and plastic model.

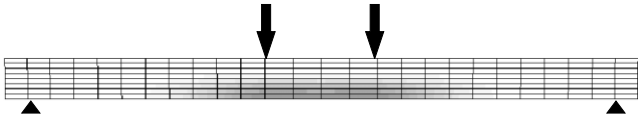

Fig. 36. Development of the hardening variable in tension.

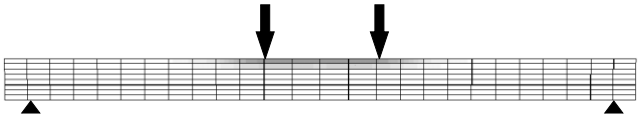

Fig. 37. Development of the hardening variable in compression.

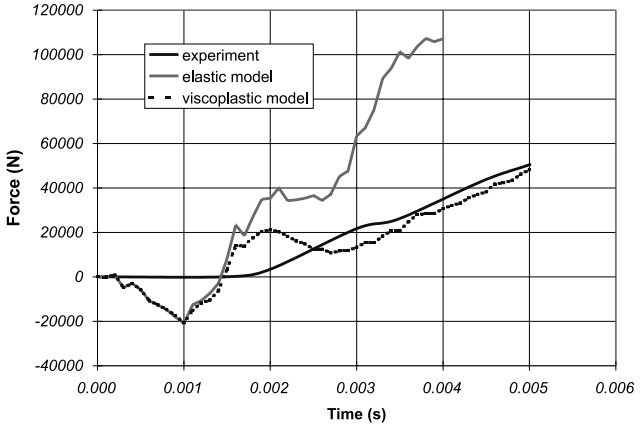

Fig. 38. Force in left support against time.

more reliable than the result given by the elastic model as we can notice in Fig. 38. Stresses given by the elastic calculation are higher and unrealistic. Moreover, a difference between the elastic or viscoplastic model response and the experiment results is observed until the time 0.002 s. Firstly, in the calculation, we have assumed that the supports were infinitesimally rigid in contrast to the experiment, where the beam presented a free vertical displacement at the beginning of the test. Secondly, we think that a viscoelastic–viscoplastic model would be more efficient to predict the beam behaviour. Indeed, an elastic behaviour which describes a non-dispersive medium does not lead to an accurate prediction of the wave propagation velocity. We experimentally observe that viscous effects are really present within the elastic domain before the plastic or damage evolution [18].

A calculation with another viscosity parameter was carried out ($\eta = 10^{-6}$). We concluded that the modification of the viscosity parameter does not change the deflection curve. Nevertheless, we observed that the viscosity parameter and the length scale govern the failure process and particularly the width of the damage zone.

6. Conclusions

The strength of concrete increases when strain rate increases. It remains difficult to dissociate effectively the rate effect from the inertial one, and in our opinion the major experimental attempts to assess this phenomenon have failed thus far. This issue is related to the fact that the experimental apparatus is not yet able to capture the desired phenomenon, that is the concrete material dynamic behaviour, and shows the influence of boundary conditions. The numerical results reported in this paper with a viscoplastic hydrostatic pressure-dependent model showed differences between the impact and static behaviour of plain concrete loaded in uniaxial compression. Therefore, the modeling could constitute an alternative not in order to predict the material response, but to try to understand and to evaluate the rate effect. The numerical simulations of the SHPB test gives an idea about the dynamic concrete behaviour. They especially demonstrate in a prominent manner the contribution of the forces of inertia, inertial confinement, structural effect and rate effect on the visible increase in strength of a specimen under compression. The viscosity which is present in the model can be used on one hand to model this rate effect and on the other hand to bring in the motion equation the terms permitting the development of the localized zone. Indeed, the failure process by localization of deformations can be approached with a viscoplastic model. The viscosity parameter is based on the internal length scale. After the material response validation, the model was used in the simulation of a structure under dynamic loading. Calculation on a beam subjected to impact gave results which are in good agreement with experimentally measured forces and deflections. Nevertheless, it seems that the concrete behaviour would have to be considered as viscoelastic–viscoplastic in order to improve the model prediction.

Acknowledgements

The authors are very grateful to the network "Géomatériaux" for providing the experimental data and for its help in accomplishing this study.

References

[1] Bailly P. Modélisation des essais de compression dynamique. GRECO 1992.
[2] Bischoff PH, Perry SH. Compressive behaviour of concrete at high strain rates. Mater Struct 1991;24:425–50.
[3] Bischoff PH, Perry SH. Impact behavior of plain concrete loaded in uniaxial compression. J Eng Mech Div, ASCE 1995;121(6).
[4] Charas T, Millard A, Verpeaux P. Solution of 2D and 3D contact problems by mean of Lagrange multipliers in the CASTEM 2000 finite element program. In: Proceedings of the Conference on Contact Mech. New York: Comput. Mech. Pub; 1993. p. 183–94.
[5] Criesfield MA, Wills J. Analysis of R/C Panels using different concrete models. J Eng Mech Div, ASCE 1989;115(3).
[6] Dubé JF, Pijaudier-Cabot G, La C. A rate-dependent damage model for concrete in dynamics. J Eng Mech Div, ASCE 1996; 122(10).
[7] Eibel M, Lohrmann G. Verification experiments on FRC structural elements: Dynamic loading. Report on Subtask BE-89-3275 1993, University of Karlsruhe, 43 p.
[8] Feenstra HP. Computational aspects of biaxial stress in plain and reinforced concrete. Ph.D thesis. Delft University, 1993.
[9] Gary G. Essais à grande vitesse sur béton. Problèmes spécifiques. Scientifique Rapport GRECO 1990, Edité par J.M. Reynouard, France.
[10] Georgin JF, Reynouard JM, Merabet O. Localisation in modeling of structures submitted to impact by viscoplasticity. In: Proceedings of the 5th COMPLAS, Barcelona 1997.
[11] Hopkinson B. A method of measuring the pressure produced in the detonation of high explosives or by the impact of bullets. Philios Trans R Soc London, Ser A 1914;213(10):437–56.
[12] Koiter W. Stress–strain relations, uniqueness and variational theorems for elastic–plastic materials with a singular yield surface. Q Appl Math 1953;(3).
[13] Kotsovos MD. Effect of testing techniques on the post-ultimate behavior of concrete in compression. Mater Struct 1983;16:3–12.
[14] Maier G. Linear flows-laws of elastoplasticity: a unified general approach. Lincei-Rend, Sci Fis Mat Nat 1969;47:266–76.
[15] Meftah F. Contribution à l'étude numérique des modes localisés de rupture dans les structures en béton de types poutres: approche multicouches par la plasticité au gradient. PhD Thesis, INSA de LYON, 1997.
[16] Pramono E, Willam K. Implicit integration of composite yield surfaces with corners. Eng Comp 1989;6.
[17] Rossi P. Strain rate effects in concrete structures: the LCPC experience. Mater Struct 1997;00:54–62.
[18] Sercombe J, Ulm F-J, Toutlemonde F. Viscous hardening plasticity for concrete under high rate dynamic loading. J Eng Mech, ASCE 1998;124(9):1050–7.
[19] Simo JC, Kennedy JG, Govindjee S. Non-smooth multisurface plasticity and viscoplasticity. Loading/unloading conditions and numerical algorithms. Int J Numer Meth Eng 1988;26:2161–85.
[20] Sluys LJ. Wave propagation, localisation and dispersion in softenings solids. PhD thesis, Delft University, 1992.
[21] Sluys LJ, De Borst R. Computational modeling of impact tests on steel fibre reinforced concrete beams. Heron 1992;37(4):3–15.
[22] Tang T, Malvern LE, Jenkins DA. Rate effects in uniaxial dynamic compression of concrete. J Eng Mech, ASCE 1992; 118(1).
[23] Toulemonde F. Résistance au choc des structures en béton: du comportement du matériau au calcul des ouvrages. PhD thesis, ENPC, Paris 1994.
[24] Wang QB, VanDerVorm PLJ, Blaauwendraad J. Failure of reinforced concrete panels-how accurate the models must be? In: Bicanic N et al., editors. Comput Aided Anal Des Concr Struct. Swansea, UK: Pineridge Press; 1990. p. 153–63.
[25] Zhao H, Gary G. On the use of the SHPB techniques to determine the dynamic behavior of materials in the range of small strains. Int J Solids Struct 1996;33(23):3363–75.